

## Reversible control of magnetism in $\text{La}_{0.67}\text{Sr}_{0.33}\text{MnO}_3$ through chemically-induced oxygen migration

A. J. Grutter, D. A. Gilbert, U. S. Alaan, E. Arenholz, B. B. Maranville, J. A. Borchers, Y. Suzuki, Kai Liu, and B. J. Kirby

Citation: *Applied Physics Letters* **108**, 082405 (2016); doi: 10.1063/1.4942645

View online: <http://dx.doi.org/10.1063/1.4942645>

View Table of Contents: <http://scitation.aip.org/content/aip/journal/apl/108/8?ver=pdfcov>

Published by the AIP Publishing

---

### Articles you may be interested in

[Tunnelling anisotropic magnetoresistance at  \$\text{La}\_{0.67}\text{Sr}\_{0.33}\text{MnO}\_3\$ -graphene interfaces](#)

*Appl. Phys. Lett.* **108**, 112405 (2016); 10.1063/1.4942778

[Magnetic anisotropy and magnetization reversal of  \$\text{La}\_{0.67}\text{Sr}\_{0.33}\text{MnO}\_3\$  thin films on  \$\text{SrTiO}\_3\$  \(110\)](#)

*J. Appl. Phys.* **108**, 103906 (2010); 10.1063/1.3506407

[Magnetization reversal mechanism in  \$\text{La}\_{0.67}\text{Sr}\_{0.33}\text{MnO}\_3\$  thin films on  \$\text{NdGaO}\_3\$  substrates](#)

*J. Appl. Phys.* **107**, 013904 (2010); 10.1063/1.3273409

[Rotation of the magnetic easy axis in  \$\text{La}\_{0.67}\text{Sr}\_{0.33}\text{MnO}\_3\$  thin film on  \$\text{NdGaO}\_3\$  \(112\)](#)

*Appl. Phys. Lett.* **94**, 042502 (2009); 10.1063/1.3074445

[Reversible electroresistance at the  \$\text{Ag}/\text{La}\_{0.67}\text{Sr}\_{0.33}\text{MnO}\_3\$  interface](#)

*J. Appl. Phys.* **100**, 033704 (2006); 10.1063/1.2222069

---

The advertisement features a photograph of the Lake Shore Model 372 cryogenic temperature controller, a white rectangular device with a digital display and control buttons. To the right, a detailed view of a cryogenic system's internal components, including a cryostat and various sensors, is shown. The Lake Shore CRYOTRONICS logo is positioned in the upper right corner of the image.

Precise temperature control  
for cryogenic research

Model 372

Lake Shore  
CRYOTRONICS



# Reversible control of magnetism in $\text{La}_{0.67}\text{Sr}_{0.33}\text{MnO}_3$ through chemically-induced oxygen migration

A. J. Grutter,<sup>1,a),b)</sup> D. A. Gilbert,<sup>1,a),b)</sup> U. S. Ala'an,<sup>2,3</sup> E. Arenholz,<sup>4</sup> B. B. Maranville,<sup>1</sup> J. A. Borchers,<sup>1</sup> Y. Suzuki,<sup>3,5</sup> Kai Liu,<sup>6</sup> and B. J. Kirby<sup>1</sup>

<sup>1</sup>NIST Center for Neutron Research, National Institute of Standards and Technology, Gaithersburg, Maryland 20899, USA

<sup>2</sup>Department of Materials Science and Engineering, Stanford University, Stanford, California 94305, USA

<sup>3</sup>Geballe Laboratory for Advanced Materials, Stanford University, Stanford, California 94305, USA

<sup>4</sup>Advanced Light Source, Lawrence Berkeley National Laboratory, Berkeley, California 94720, USA

<sup>5</sup>Department of Applied Physics, Stanford University, Stanford, California 94305, USA

<sup>6</sup>Department of Physics, University of California, Davis, California 95616, USA

(Received 18 December 2015; accepted 9 February 2016; published online 24 February 2016)

We demonstrate reversible control of magnetization and anisotropy in  $\text{La}_{0.67}\text{Sr}_{0.33}\text{MnO}_3$  films through interfacial oxygen migration. Gd metal capping layers deposited onto  $\text{La}_{0.67}\text{Sr}_{0.33}\text{MnO}_3$  leach oxygen from the film through a solid-state redox reaction to form porous  $\text{Gd}_2\text{O}_3$ . X-ray absorption and polarized neutron reflectometry measurements show Mn valence alterations consistent with high oxygen vacancy concentrations, resulting in suppressed magnetization and increased coercive fields. Effects of the oxygen migration are observed both at the interface and also throughout the majority of a 40 nm thick film, suggesting extensive diffusion of oxygen vacancies. After Gd-capped  $\text{La}_{0.67}\text{Sr}_{0.33}\text{MnO}_3$  is exposed to atmospheric oxygen for a prolonged period of time, oxygen diffuses through the  $\text{Gd}_2\text{O}_3$  layer and the magnetization of the  $\text{La}_{0.67}\text{Sr}_{0.33}\text{MnO}_3$  returns to the uncapped value. These findings showcase perovskite heterostructures as ideal candidates for developing functional interfaces through chemically-induced oxygen migration. © 2016 AIP Publishing LLC.

[<http://dx.doi.org/10.1063/1.4942645>]

In the search for functional magnetic and magnetoelectric interfaces, there has been a recent surge of interest in controlling magnetic properties by engineering the oxygen stoichiometry. Exciting results have been achieved in thin film heterostructures through the pairing of highly defective  $\text{GdO}_x$  layers with ultrathin layers of ferromagnetic metals such as Co.<sup>1-4</sup> Recent work has shown that high oxygen mobility in defective  $\text{GdO}_x$  facilitates oxygen transport near the interface and allows modification of the Co magnetic properties.<sup>1-4</sup> Oxygen migration in  $\text{GdO}_x/\text{Co}$  bilayers was shown to be reversibly driven by a low-power voltage pulse, suggesting electrically induced oxygen migration as a promising route towards achieving functional magnetoelectric devices.

It is well known that the magnetic ground states of complex oxide systems such as perovskites are highly sensitive to changes in valence.<sup>5-9</sup> In fact, the tunability of these complex oxides through strain, oxygen stoichiometry, and electronic structure has placed them among the most attractive materials for the stabilization of functional magnetic interfaces.<sup>5,6,10-16</sup> Many perovskites, including  $\text{La}_{0.67}\text{Sr}_{0.33}\text{MnO}_3$  (LSMO), exhibit the high oxygen mobility that makes the  $\text{GdO}_x/\text{Co}$  system so successful.<sup>17-22</sup> It is likely, therefore, that the deposition of a strongly reducing Gd film on an oxide with high oxygen mobility will induce significant oxygen migration and alter the magnetic properties.<sup>23-25</sup> We may exploit this to engineer the magnetic properties of extremely thin functional interfaces.

In this letter, we probe the magnetic properties of Gd-capped LSMO films as a function of Gd film thickness. Characterization with vibrating sample magnetometry (VSM) and X-ray magnetic circular dichroism (XMCD) shows suppression of the LSMO saturation magnetization and increased magnetic coercivity, with both effects increasing with Gd thickness. Polarized neutron reflectometry (PNR) and X-ray absorption (XA) spectroscopy measurements reveal depleted oxygen content of the LSMO extending from the interface, where the effect is the strongest, through the majority of a 40 nm thick film. Rather than providing a mobile oxygen supply as in the  $\text{GdO}_x/\text{Co}$  system, the metallic Gd layer in this case reduces the LSMO to form a porous layer of  $\text{Gd}_2\text{O}_3$ . We show that the changes are reversible, with prolonged exposure to atmospheric oxygen restoring the magnetic and electronic properties of uncapped LSMO. Both the depleted oxygen content in Gd/LSMO bilayers and the recovery of the initial (uncapped) properties over time are indications that oxygen may be readily redistributed through the entire stack.

Each 40 nm thick LSMO film was deposited on single-crystal (001)  $\text{SrTiO}_3$  using pulsed laser ablation with a fluence of  $1.4 \text{ J cm}^{-2}$  at  $700^\circ\text{C}$  in 43 Pa of  $\text{O}_2$ . LSMO films were co-deposited in pairs, with one sample retained as an uncapped control while the other was capped with Gd. After breaking vacuum, the Gd layer was deposited using electron-beam evaporation in a vacuum chamber with a base pressure of  $2.7 \times 10^{-4} \text{ Pa}$ . The Gd layer thickness was monitored using a quartz crystal oscillator, and nominal thicknesses of 0.2 nm, 0.8 nm, and 10 nm were used in this study. Actual

<sup>a)</sup>Authors to whom correspondence should be addressed: Electronic addresses: alexander.grutter@nist.gov and dustin.gilbert@nist.gov

<sup>b)</sup>A. J. Grutter and D. A. Gilbert contributed equally to this work.

measured thicknesses may deviate from nominal values due to absorption of oxygen from the LSMO and the formation of porous  $\text{Gd}_2\text{O}_3$  layers. Prior to initial VSM, PNR, XA, and XMCD measurements, samples were stored under vacuum, after which they were exposed to atmospheric oxygen for 213 days and recharacterized. To ensure that the conditions of the Gd deposition did not influence the LSMO film, we fabricated a control sample for which the Gd was instead deposited through room temperature sputtering. We find excellent agreement between the properties of this sample and those deposited through evaporation. For a full discussion, see the supplementary information.<sup>26</sup>

Room temperature VSM measurements for all three Gd thicknesses and the corresponding as-grown samples are shown in Figure 1. As can clearly be seen, 0.2 nm of Gd does not appreciably alter the magnetic properties of the LSMO film. In contrast, the deposition of 0.8 nm of Gd reduces the saturation magnetization by 9%. Increasing the Gd thickness to 10 nm further suppresses the saturation magnetization to a total of 18%. Additionally, this sample shows an increase in coercive field, from 0.24 mT to 0.46 mT. Although uncapped films from different growths show very little deviation in saturation magnetization, there is some batch-to-batch variation which manifests as differences in coercive field. These differences likely result from minor inconsistencies in laser spot size and thermal contact between growths, but appear to affect co-deposited samples identically.

Having demonstrated that a thin Gd layer alters the magnetic properties of the LSMO, we performed grazing ( $30^\circ$ ) incidence room temperature XA and XMCD measurements in an applied field of  $\pm 500$  mT to determine the effect of the Gd layer on the Mn oxidation state. Measuring the total electron yield (TEY) signal, with an expected electron escape depth of 3–5 nm, we obtain high-resolution spectroscopy of the Mn L-edge at the LSMO/Gd interface near the sample surface.<sup>27</sup> We will focus here on samples with and without a 0.8 nm Gd

capping layer. However, similar results are obtained for the 10 nm Gd cap. Both XA and XMCD measurements of uncapped and 0.8 nm Gd-capped samples are shown in Figures 1(d) and 1(e), respectively. The XA and XMCD have been background subtracted and normalized such that the Mn  $L_3$  absorption peaks have equal area. The XA spectra of the uncapped LSMO film are consistent with the mixed  $\text{Mn}^{3+}$  and  $\text{Mn}^{4+}$  valence expected in LSMO films, with a weak shoulder peak which may indicate a small amount of strain induced oxygen vacancy formation near the LSMO surface.<sup>28–32</sup> Such peaks are commonly observed in LSMO films, and this peak is greatly enhanced in the Gd capped sample, which shows a sharp deviation in the XA lineshape. Based on the position and increased intensity of this  $L_3$  shoulder peak, we conclude that additional oxygen vacancies are formed and a significant fraction of the interfacial Mn is in the 2+ valence state.<sup>31–35</sup> The main  $L_3$  peak ( $E \approx 641$  eV) is also shifted to slightly lower energy, indicating movement from mixed  $\text{Mn}^{3+}$  and  $\text{Mn}^{4+}$  to pure  $\text{Mn}^{3+}$ .<sup>33–35</sup> The decreased relative intensity of the  $L_2$  edge for Gd-capped samples is consistent with this interpretation.<sup>33–35</sup>

In agreement with bulk magnetometry, XMCD shows reduced magnetization associated with the presence of a Gd capping layer. Specifically, the integrated dichroism under the Mn  $L_3$  edge corresponds to a 21% reduction in LSMO magnetization for the 0.8 nm Gd-capped sample, larger than the 9% average magnetization reduction obtained from VSM measurements. Since TEY measurements are surface sensitive, this 21% reduction likely originates in a region of the LSMO film near the LSMO/Gd interface. If this region is assumed to have a uniform 21% reduction in magnetization, then it must be thicker than 16 nm ( $\geq 40\%$  of the total LSMO thickness) in order to give rise to an average magnetization reduction of 9%. Alternatively, the magnitude of the effect may decay slowly with increasing depth, and the entirety of the film may be affected. To probe the contribution of the Gd layer to the magnetization, we also performed both XA and XMCD measurements on the Gd  $M^{4,5}$  edge.<sup>26</sup> The XA measurements show excellent agreement with the  $\text{Gd}^{3+}$  oxidation state, while room temperature XMCD measurements show no significant dichroism, even at fields of  $\pm 500$  mT, indicating that the magnetization originates exclusively in the LSMO.<sup>26,36</sup>

Thus, we have demonstrated that depositing a Gd capping layer onto a LSMO film suppresses the LSMO magnetization and induces a change in Mn valence at the interface. Furthermore, X-ray and VSM measurements suggest that the effects of the Gd layer are not confined exclusively to the interface. To determine the thickness dependence of the magnetization and structure, we performed PNR using the PBR and MAGIK instruments at the NIST Center for Neutron Research. We examined the non-spin-flip scattering channels, in which incident and scattered neutrons were polarized either spin-up or spin-down with respect to the applied in-plane magnetic field (17 mT). The specular reflectivity of spin-polarized neutrons depends on the depth profile of both the nuclear composition and the sample magnetization parallel to the applied field. Unlike the other sample components, Gd is a strong neutron absorber, which must be accounted for in the modeling through the inclusion of an imaginary scattering

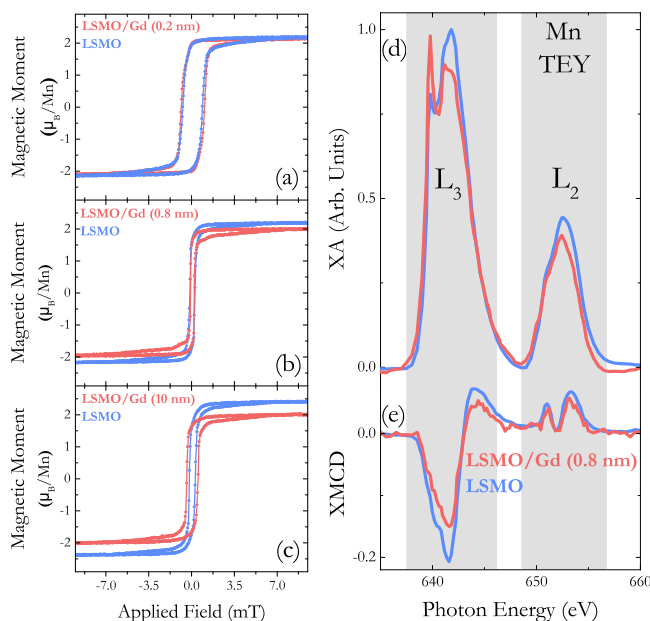


FIG. 1. Major hysteresis loops of capped and uncapped films for Gd layer thicknesses of (a) 0.2 nm, (b) 0.8 nm, and (c) 10 nm. (d) TEY XA and (e) XMCD spectra of the samples shown in panel (b).

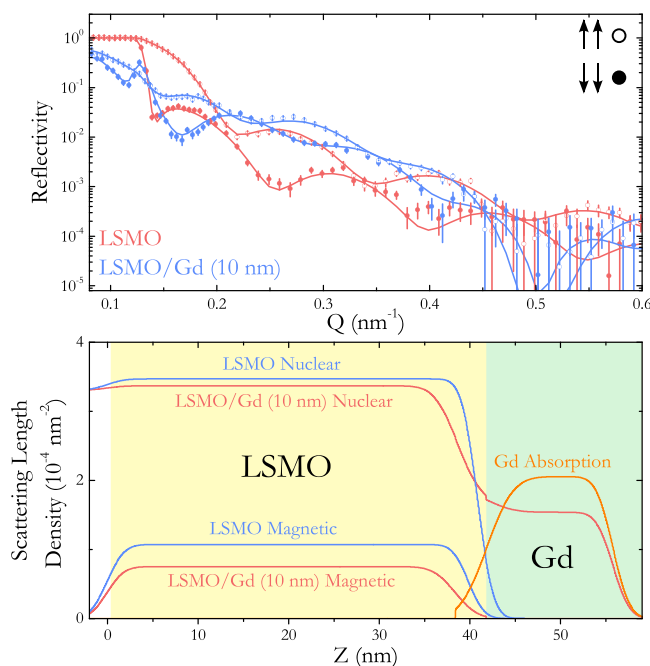


FIG. 2. (Top) Non-spin-flip PNR for a bare LSMO film alongside one capped by 10 nm of Gd in an applied field of 17 mT. Error bars correspond to  $\pm 1$  standard deviation. (Bottom) Nuclear, magnetic, and imaginary SLD profiles used to generate the fits shown.

length density (SLD) in the capping layer. PNR data were modeled using the Refl1D software package.<sup>26,37</sup>

PNR of a capped/uncapped sample pair for a nominal Gd thickness of 10 nm is shown in Figure 2(top) as circles alongside a theoretical fit to the data (line), while Figure 2(bottom) shows the models used to fit the data. As expected, the thicknesses of the LSMO layers match extremely well. However, the SLD profiles of the LSMO layer show significant differences. Specifically, the Gd-capped LSMO layer has a reduced nuclear SLD near the LSMO/Gd interface, along with a smaller reduction in the bulk. This change indicates oxygen removal from the LSMO layer of the Gd-capped film, with fitted SLDs corresponding to  $\text{La}_{0.67}\text{Sr}_{0.33}\text{MnO}_{2.89}$  and  $\text{La}_{0.67}\text{Sr}_{0.33}\text{MnO}_{1.46}$  in the bulk and interfacial LSMO, respectively.<sup>26</sup> The reduced oxygen content is associated with suppression of the magnetization near the LSMO/Gd interface and a general reduction in magnetization throughout the film. Given the large changes in bulk magnetization with such a small change in oxygen content, we estimate that a single nanometer of Gd could affect as much as 18 nm of LSMO.<sup>26</sup>

The fit shown represents the best solution based on the models used; as with all scattering techniques, there may be other models which generate the same intensity data, but we can exclude specific competing models that might otherwise be considered physical.<sup>26</sup> In addition, we note that samples with highly neutron absorbing layers are susceptible to fitting artifacts that may alter the perceived film roughness. We therefore base our conclusions primarily on SLD and thickness, rather than interfacial roughness. We represent the sample as series of slab-like layers with Gaussian roughness at the interfaces, with a separate layer representing a region of additional oxygen depletion near the interface. Models restricting the magnetization of the bulk LSMO to be constant between the two states, or with invariant oxygen content, yielded

significantly worse fits.<sup>26</sup> We conclude, therefore, that the sample forms a 3.4(2) nm thick interfacial region which is nonmagnetic and highly oxygen depleted, while the majority of the film is slightly oxygen deficient and exhibits sharply reduced magnetization. The reduction in the integrated magnetic SLD is in excellent agreement with the reduction in the magnetization from VSM measurements.

After the initial measurements, samples with 10 nm Gd caps were exposed to atmospheric  $\text{O}_2$  levels for 213 days, after which VSM, XAS, XMCD, and PNR characterization was repeated. Modeling the PNR shows recovery of the LSMO nuclear and magnetic SLDs towards those of the uncapped LSMO, as illustrated in Figures 3(a) and 3(b). The Gd/LSMO interface in particular, shows an increase in nuclear SLD, with the interfacial and bulk LSMO values nearly matching. This result suggests that the oxygen content is now relatively constant throughout the LSMO layer. In addition to the magnetization increase throughout the film, we see that the oxygen depletion layer at the interface has been eliminated.

These observations are confirmed by VSM, XAS, and XMCD. VSM measurements of the same sample, shown in Figure 3(c), indicate excellent agreement between saturation magnetization and coercive field for aged capped and uncapped films. Fluorescence yield (FY) XA and XMCD measurements, shown in Figure 3(d), penetrate the Gd capping layer to probe the entire LSMO layer, but are distorted due to self-absorption effects.<sup>27</sup> Qualitatively, we find that the capped and uncapped films have nearly identical valence states, as demonstrated by matching XA lineshapes, and magnetizations, as shown by extremely well-matched XMCD magnitude and lineshapes. Therefore, we conclude that exposure to atmospheric  $\text{O}_2$  results in a recovery of the valence, magnetic properties, and structure of the uncapped LSMO film.

It is now clear that the deposition of a Gd capping layer may be used to significantly alter the magnetic properties of complex oxide thin films. Based on the XA and PNR measurements, we propose that upon deposition, a Gd capping layer rapidly extracts oxygen from the LSMO layer, forming a layer of  $\text{Gd}_2\text{O}_3$ . This loss of oxygen from the LSMO is energetically favorable, due to the strongly reducing nature of Gd and the flexible valence state of Mn. Thus, an oxygen poor region is formed in the interfacial LSMO, resulting in concentrated oxygen vacancies, structural distortions, and the stabilization of  $\text{Mn}^{2+}$ . All of these deviations from ideal LSMO stoichiometry and structure act to suppress the magnetization at the interface. Due to the high mobility of oxygen vacancies in perovskite oxide thin films such as LSMO, a significant fraction of the vacancies diffuse away from the interface and the bulk magnetization is substantially suppressed.

Reintroduction of atmospheric oxygen can be understood through the porosity of the  $\text{Gd}_2\text{O}_3$  layer. The measured nuclear SLD, as extracted from PNR, is only 56% of the expected value of bulk crystal  $\text{Gd}_2\text{O}_3$ . However, a porous layer is consistent with the reduced SLD and allows oxygen transport through the capping layer. The oxygen-depleted LSMO layer absorbs atmospheric oxygen, which then diffuses throughout the system and restores the properties to the as-grown condition. Additional evidence for this explanation

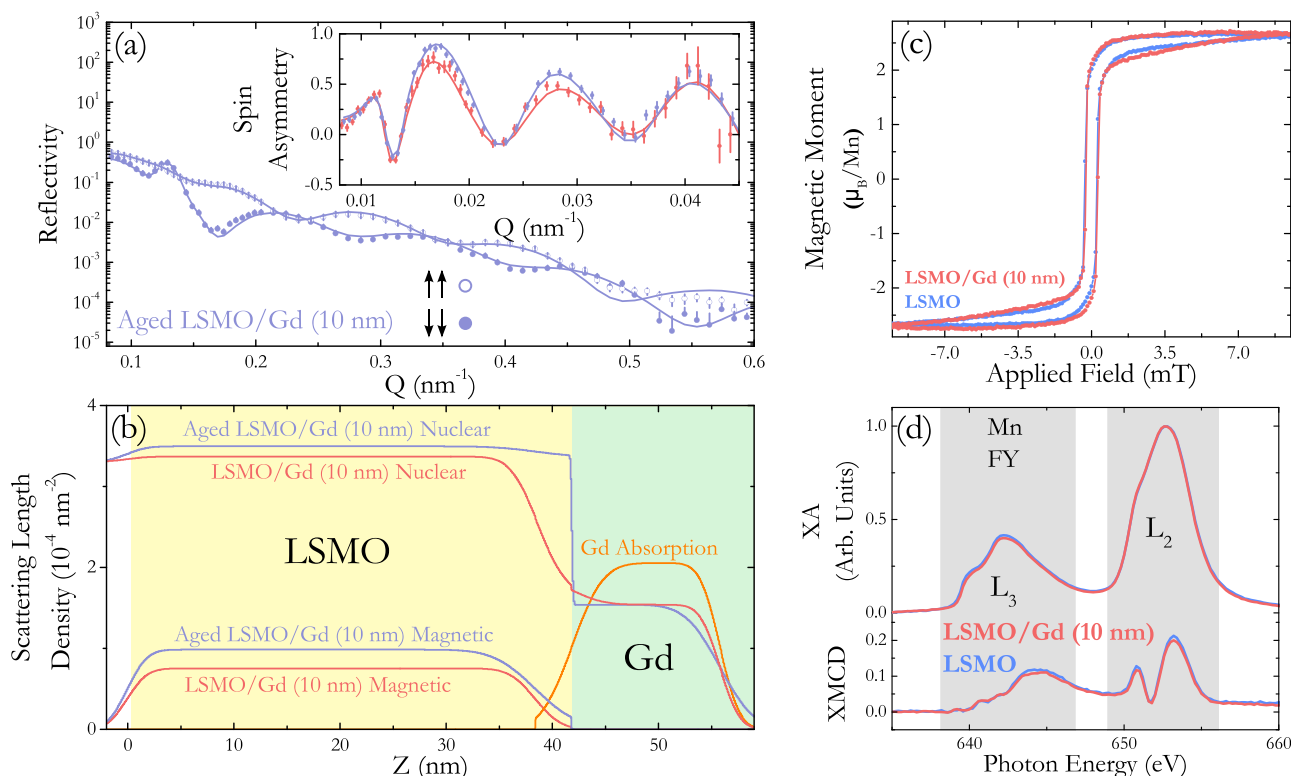


FIG. 3. (a) PNR measurement and theoretical fit for the 10 nm Gd-capped sample shown in Figure 2 after aging in atmospheric  $O_2$ . PNR was performed at 300 K in an applied field of 17 mT. (Inset) Spin asymmetry and theoretical fits of the sample before and after aging. (b) Nuclear, magnetic, and imaginary SLDs used to generate the fits shown. (c) VSM, (d) FY XA, and XMCD measurements after aging alongside the corresponding uncapped LSMO film.

can be found through examination of trends in the coercive fields of the films. Although a 10 nm Gd capping layer increases the coercive field of the LSMO, the magnetization reversal remains sharp, and the coercive field reverts to the as-grown value after oxygen re-absorption. We propose that the increased coercivity originates in the development of additional domain wall pinning sites through the high density of induced defects. Once these defects have been eliminated through oxygen absorption, the domain walls are once again free to propagate at lower applied fields.

Through this study, we have implemented a relatively unexplored route towards reversible control of valence and magnetism in perovskite heterostructures. Although the largest effect appears to be localized at the interface, it is significant that major changes in the properties of the whole film are observed. In particular, extraction of oxygen from the entire film implies that these systems exhibit the high oxygen mobility which is desirable for room temperature spintronic applications. Given the sensitivity of magnetic properties in LSMO and other complex oxides to changes in valence, it is clear that perovskite heterostructures are ideal systems in which to stabilize functional interfaces through chemical migration. Enabled by the high degree of oxygen vacancy conduction exhibited by these materials, chemically induced oxygen migration offers exciting pathways towards control of magnetic oxide interfaces.

A.J.G and D.A.G. acknowledge support from the NRC Research Associateship Program. U.S.A. acknowledges support from the Army Research Office (W911NF-14-1-0611). Y.S. and K.L. acknowledge support from the National Science Foundation (DMR-1402685 and DMR-1543582,

respectively). The Advanced Light Source is supported by the Director, Office of Science, Office of Basic Energy Sciences, of the U.S. Department of Energy under Contract No. DE-AC02-05CH11231.

- <sup>1</sup>U. Bauer, L. Yao, A. J. Tan, P. Agrawal, S. Emori, H. L. Tuller, S. Van Dijken, and G. S. Beach, *Nat. Mater.* **14**, 174 (2015).
- <sup>2</sup>U. Bauer, S. Emori, and G. Beach, *Appl. Phys. Lett.* **101**, 172403 (2012).
- <sup>3</sup>U. Bauer, S. Emori, and G. Beach, *Appl. Phys. Lett.* **100**, 192408 (2012).
- <sup>4</sup>C. Bi, Y. Liu, T. Newhouse-Illige, M. Xu, M. Rosales, J. W. Freeland, O. Mryasov, S. Zhang, S. G. E. te Velthuis, and W. G. Wang, *Phys. Rev. Lett.* **113**, 267202 (2014).
- <sup>5</sup>P. Orgiani, A. Yu. Petrov, R. Ciancio, A. Galdi, L. Maritato, and B. A. Davidson, *Appl. Phys. Lett.* **100**, 042404 (2012).
- <sup>6</sup>J. Sakai, N. Ito, and S. Imai, *J. Appl. Phys.* **99**, 08Q318 (2006).
- <sup>7</sup>C. He, A. J. Grutter, M. Gu, N. D. Browning, Y. Takamura, B. J. Kirby, J. A. Borchers, J. W. Kim, M. R. Fitzsimmons, X. Zhai, V. V. Mehta, F. J. Wong, and Y. Suzuki, *Phys. Rev. Lett.* **109**, 197202 (2012).
- <sup>8</sup>R. P. Haggerty and R. Seshadri, *J. Phys.: Condens. Matter* **16**, 6477 (2004).
- <sup>9</sup>L. E. Hueso, F. Rivadulla, R. D. Sánchez, D. Caeiro, C. Jardón, C. Vázquez-Vázquez, J. Rivas, and M. A. López-Quintela, *J. Magn. Magn. Mater.* **189**, 321 (1998).
- <sup>10</sup>S. J. May, A. B. Shah, S. G. E. te Velthuis, M. R. Fitzsimmons, J. M. Zuo, X. Zhai, J. N. Eckstein, S. D. Bader, and A. Bhattacharya, *Phys. Rev. B* **77**, 174409 (2008).
- <sup>11</sup>A. Bhattacharya, S. J. May, S. G. E. te Velthuis, M. Warusawithana, X. Zhai, B. Jiang, J.-M. Zuo, M. R. Fitzsimmons, S. D. Bader, and J. N. Eckstein, *Phys. Rev. Lett.* **100**, 257203 (2008).
- <sup>12</sup>J. Hoffman, I. C. Tung, B. B. Nelson-Cheeseman, M. Liu, J. W. Freeland, and A. Bhattacharya, *Phys. Rev. B* **88**, 144411 (2013).
- <sup>13</sup>J. Chakhalian, J. W. Freeland, G. Srajer, J. Stremper, G. Khaliullin, J. C. Cezar, T. Charlton, R. Dalgliesh, C. Bernhard, G. Cristiani, H.-U. Habermeier, and B. Keimer, *Nat. Phys.* **2**, 244 (2006).
- <sup>14</sup>M. Gibert, P. Zubko, R. Scherwitzl, J. Iñiguez, and J.-M. Triscone, *Nat. Mater.* **11**, 195 (2012).

- <sup>15</sup>A. J. Grutter, H. Yang, B. J. Kirby, M. R. Fitzsimmons, J. A. Aguiar, N. D. Browning, C. A. Jenkins, E. Arenholz, V. V. Mehta, U. S. Alaan, and Y. Suzuki, *Phys. Rev. Lett.* **111**, 087202 (2013).
- <sup>16</sup>A. J. Grutter, F. J. Wong, C. A. Jenkins, E. Arenholz, A. Vailionis, and Y. Suzuki, *Phys. Rev. B* **88**, 214410 (2013).
- <sup>17</sup>M. Nord, P. E. Vullum, M. Moreau, J. E. Boschker, S. M. Selbach, R. Holmestad, and T. Tybell, *Appl. Phys. Lett.* **106**, 041604 (2015).
- <sup>18</sup>J. Garcia-Barriocanal, A. Rivera-Calzada, M. Varela, Z. Sefrioui, E. Iborra, C. Leon, S. J. Pennycook, and J. Santamaria, *Science* **321**, 676 (2008).
- <sup>19</sup>H. T. Yi, T. Choi, S. G. Choi, Y. S. Oh, and S.-W. Cheong, *Adv. Mater.* **23**, 3403 (2011).
- <sup>20</sup>R. Al-Hamadany, J. P. Goss, P. R. Briddon, S. A. Mojarad, M. Al-Hadidi, A. G. O'Neill, and M. J. Rayson, *J. Appl. Phys.* **113**, 024108 (2013).
- <sup>21</sup>J. Park, D.-H. Kwon, H. Park, C. U. Jung, and M. Kim, *Appl. Phys. Lett.* **105**, 183103 (2014).
- <sup>22</sup>R. Buzio, A. Gerbi, A. Gadaleta, L. Anghinolfi, F. Bisio, E. Bellingeri, A. S. Siri, and D. Marrè, *Appl. Phys. Lett.* **101**, 243505 (2012).
- <sup>23</sup>T. Mairoser, J. A. Mundy, A. Melville, D. Hodash, P. Cueva, R. Held, A. Glavic, J. Schubert, D. A. Muller, D. G. Schlom, and A. Schmehl, *Nat. Commun.* **6**, 7716 (2015).
- <sup>24</sup>H. D. Ramsbottom and D. P. Hampshire, *J. Appl. Phys.* **85**, 3732 (1999).
- <sup>25</sup>J. C. Park, S. W. Kim, C. J. Kim, and H.-N. Lee, *IEEE Electron Device Lett.* **33**, 809 (2012).
- <sup>26</sup>See supplementary material at <http://dx.doi.org/10.1063/1.4942645> for additional details of the Gd capping layer deposition, X-ray measurements, and polarized neutron reflectometry analysis.
- <sup>27</sup>S. Eisebitt, T. Böske, J.-E. Rubensson, and W. Eberhardt, *Phys. Rev. B* **47**, 14103 (1993).
- <sup>28</sup>G. Subías, J. García, M. C. Sánchez, J. Blasco, and M. G. Proietti, *Surf. Rev. Lett.* **9**, 1071 (2002).
- <sup>29</sup>R. V. Chopdekar, E. Arenholz, and Y. Suzuki, *Phys. Rev. B* **79**, 104417 (2009).
- <sup>30</sup>Y. Takamura, R. V. Chopdekar, E. Arenholz, and Y. Suzuki, *Appl. Phys. Lett.* **92**, 162504 (2008).
- <sup>31</sup>B. Cui, C. Song, F. Li, G. Y. Wang, H. J. Mao, J. J. Peng, F. Zeng, and F. Pan, *Sci. Rep.* **4**, 4206 (2014).
- <sup>32</sup>M. Galbiati, S. Tatay, S. Delprat, C. Barraud, V. Cros, E. Jacquet, F. Coloma, F. Choueikani, E. Otero, P. Ohresser *et al.*, *Appl. Surf. Sci.* **353**, 24 (2015).
- <sup>33</sup>R. Qiao, T. Chin, S. J. Harris, S. Yan, and W. Yang, *Curr. Appl. Phys.* **13**, 544 (2013).
- <sup>34</sup>H. K. Schmid and W. Mader, *Micron* **37**, 426 (2006).
- <sup>35</sup>Z. L. Wang, J. S. Yin, and Y. D. Jiang, *Micron* **31**, 571 (2000).
- <sup>36</sup>A. R. H. Preston, B. J. Ruck, W. R. L. Lambrecht, L. F. J. Piper, J. E. Downes, K. E. Smith, and H. J. Trodahl, *Appl. Phys. Lett.* **96**, 032101 (2010).
- <sup>37</sup>B. J. Kirby, P. A. Kienzle, B. B. Maranville, N. F. Berk, J. Krycka, F. Heinrich, and C. F. Majkrzak, *Curr. Opin. Colloid Interface Sci.* **17**, 44 (2012).